Characterization of the cuneiform signs by the use of a multifunctional optoelectronic device

Nazif Demoli, Hartmut Gruber, Uwe Dahms, and Günther Wernicke

The cuneiform-inscription (CI) signs recorded on the original clay tablet known as HS 158b from Nippur (1329 B.C.) have been characterized by the use of a multifunctional optoelectronic device. Properties such as features in object and Fourier space or similarity measures between the CI sign samples were investigated by the application of various numerical and experimental procedures. An overall algorithm of the experimental work is given, and the corresponding particular steps are described. For describing the objects from the CI font numerically, a mathematical model is introduced. To decrease the sensitivity between different samples of a sign (in-class objects) and to increase the discrimination of other signs (out-of-class objects), we designed and implemented, besides digital techniques, a coherent optical technique for averaging a training set of in-class objects. The preliminary correlation experiments conducted on several CI signs illustrate the usefulness of the proposed approach.

Key words: Optical character recognition, correlation filters, coherent optical averaging.

1. Introduction

Character reading was often a matter of concern in the field of optical pattern recognition, first as a demonstrative example,[1] and later for problems in reading, for example, the ancient handwritten Hebraic characters.[2] More recently, for handwriting recognition, a hybrid incoherent optical processor was made that computes moments of images in real time.[3] For handwritten-signature verification, the synthetic-discriminant-function approach was applied.[4] For the recognition of different styles of Chinese fonts, an optical character-recognition system using accumulated-stroke features has been developed.[5] Clay tablets that carry messages from the ancient times in the form of cuneiform inscription (CI) have been recently analyzed.[6–8]

The preliminary studies of clay tablets were concerned with investigating the possibility of the utilization of holographic techniques for high-resolution recording and for characterizing the CI font. The original CI signs are three-dimensional (3-D) objects composed of wedge-shaped imprints that can vary in number, size, and orientation from sign to sign.[9] The total collection of the CI tablets comprises approximately half a million pieces spread all over the world. Under present conditions, the world database of original CI tablets is endangered by natural or man-made destruction, so that the fine-structure information from many tablets is already hardly interpretable. Therefore, high-resolution archival storage[6] is of interest owing to the possibility of later retrieval of the complex 3-D information.

On the other hand, although the cracks, scratches, fractures, and other frequent unwanted artifacts can make reading, as well as classifying, very difficult, these are not the only problems concerning the interpretation of the CI matter. The CI sign fonts can vary significantly because of differing writers or writing schools, differing writing tools, or differing periods of writing. But the CI sign samples can also vary even if the objects were written by the same author, with the same tool, and on the same tablet. Therefore, the use of character-recognition methods for minimizing the sensitivity of an in-class group of objects while maximizing the discrimination ability for other objects, usually called out-of-class objects, is indispensable. An additional problem is the large number of clay-tablet pieces. Thus, an efficient method, which also involves a statistical approach, for identification, characterization, and classification of the CI signs is of interest.

N. Demoli is with the Laboratory for Coherent Optics, Institute of Physics, University of Zagreb, P.O. Box 304, Bijenička 46, 41000 Zagreb, Croatia; the other authors are with the Laboratory for Coherent Physics, Fachbereich Physik, Invalidenstrasse 110, 10115 Berlin, Germany.

Received 15 September 1995; revised manuscript received 6 May 1996.

0003-6935/96/295811-10$10.00/0

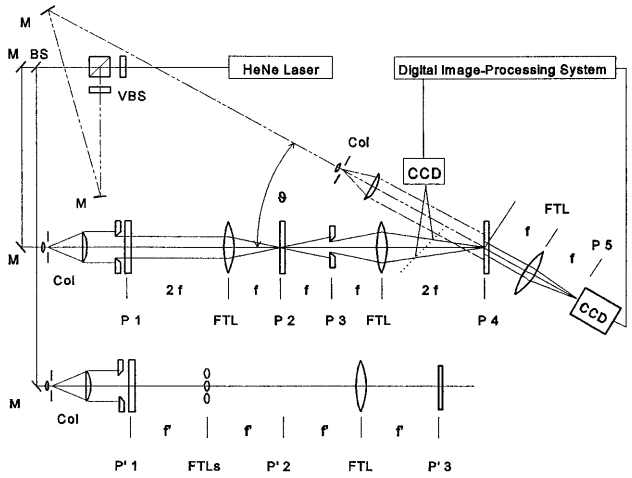

Fig. 1. Schematic diagram of the multifunctional optoelectronic system. VBS, variable beam splitter; M, mirror; Col, collimator; FTL, Fourier-transform lens.

For the characterization of the CI signs a multifunctional extended optoelectronic correlator (MEOC) device has been developed. Starting with the recognition experiments of a single wedge element typical of all CI signs,[6,7] we have carried out measurements on self-modeled 3-D scenes.[8] In this paper we present the results obtained with the CI signs from an original clay tablet. In Section 2 we describe our optical device, the preprocessing procedures including a previously introduced technique for the experimental realization of quasi-phase-only filters (QPOF's),[10] and the correlation parameters. Sections 3 and 4 are mathematically oriented. Section 3 introduces a two-dimensional (2-D) model for describing the CI signs, whereas Section 4 describes the mechanism of the coherent optical-averaging method. An overall algorithm of the experimental work is outlined in Section 5. The new CI characterization results are reported in Section 6. Finally, the conclusions drawn are outlined in Section 7.

2. Preliminaries

A. Experimental Device

An experimental device called the MEOC system was advanced, permitting the detection, Fourier analysis, feature enhancement, feature extraction, coherent optical averaging, and correlation experiments to be performed, including several preprocessing procedures. Correlation filters (CF's) are formed at plane P_4 of the system, schematically shown in Fig. 1, when the Fourier transform (FT) of a reference signal placed at plane P_1 is interfered with an off-axis collimated beam emerging from the P_4 plane under the angle ϑ. During correlation experiments the CF's were positioned at P_4, and the inputs at P_1. Planes P_2 and P_3 were used for optically prefiltering the input signals. The optical system is supported by a CCD camera and a digital image-processing (DIP) system. Placing a CCD at plane P_4 yields an extended optical Fourier analyzer system. An additional axis is used for carrying out the optical-averaging procedure.

B. Preprocessing Procedures

Optical preprocessing in the frequency space is performed at plane P_2, whereas image prefiltering is performed at plane P_3. The $3f$ distances between planes P_1 and P_2 and between planes P_3 and P_4 result from the quadratic phase factor in the FT relation. Thus, the exact FT of an input signal is obtained at plane P_4 of the system. If w_1 denotes the input aperture, W_2 the frequency–amplitude filter at P_2, and w_3 the image filter at P_3, then the modified spectrum F' of an input f is given by

$$F' = \{[F \otimes W_1]W_2\} \otimes W_3, \tag{1}$$

where the convolution operator ($\otimes$) denotes a 2-D convolution and capital letters denote the FT's of the spatial functions. From Eq. (1) it is seen that the spectrum modification can be described by the convolution of the FT of the input signal with the FT of the input aperture, multiplied by the frequency-plane spatial filter, and then followed by a further convolution with the image-plane spatial filter. The preprocessor is not only a spatial-frequency selector but also an aperture modifier. Such prefiltering is needed because, in many situations, the input information is disturbed by low-frequency contents (originating from the input aperture and unwanted artifacts like cracks, scratches, etc.) or by an additive stationary input noise.[7]

To produce high-efficiency, high-sensitivity CF's, we have used the technique for synthesizing QPOF's.[10] Lowering the maxima of the power spectrum of the reference signal was achieved with the help of an attenuation mask (AM). We can easily

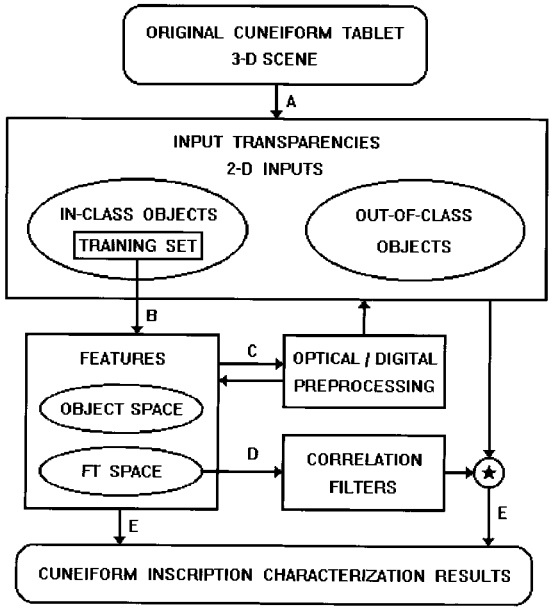

Fig. 2. Block diagram of the algorithm summarizing the experimental work.

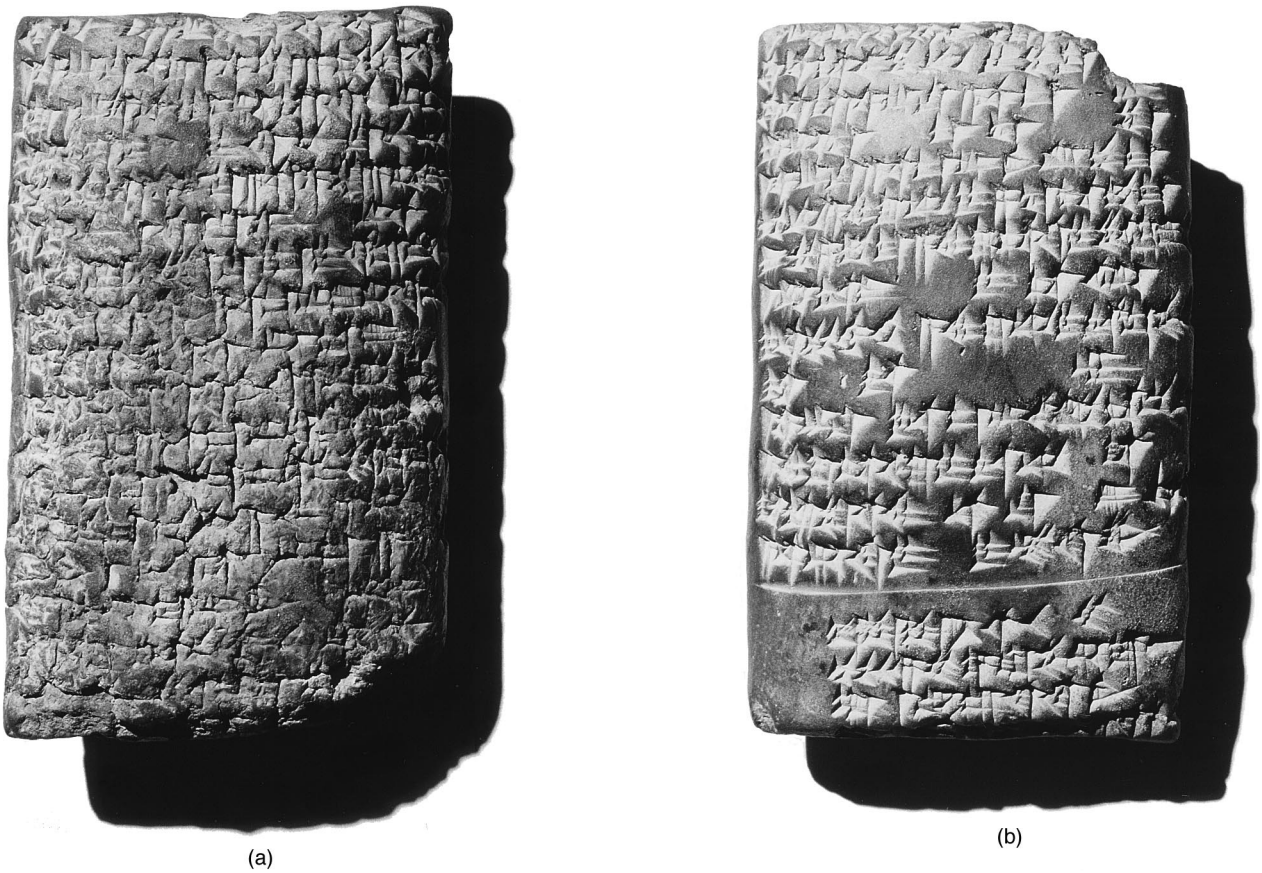

(a) (b)

Fig. 3. Photographs of the original CI tablet, HS 158b: (a) the front and (b) the back sides.

realize an AM by exposing, developing, and repositioning a photographic plate in the P_2 plane of the experimental device. Because of nonlinear recording, the low-power frequency components of input signals are practically not attenuated, whereas the power spectrum maxima are lowered to the level controlled by the AM recording parameters. The resulting negative transparency represents an ideal high-resolution frequency-plane nonlinear attenuator. This permits a full-modulation adjustment of the CF over all high-power frequency components, thus making a significant increase in the CF efficiency possible.[10]

C. Correlation Parameters

We denote the coordinates of the input, filter, and correlation planes of a standard optical correlator system by (x_i, y_i), (u, v), and (x, y), respectively. Uppercase letters are used to represent the FT of spatial functions, and $\mathrm{FT}\{\cdots\}$ denotes the FT operator. If an input $f(x_i, y_i)$ is placed at plane P_1 and the CF of a reference signal $h(x_i, y_i)$ at plane P_4 of the system shown in Fig. 1, then the amplitude of the correlation signal $c(x, y)$ at plane P_5 is given by

$$c(x, y) = \mathrm{FT}\{F'(u, v)H^*(u, v)\}, \tag{2}$$

where $F'(u, v)$ denotes the prefiltered $F(u, v)$, according to Eq. (1), and the asterisk denotes the complex conjugate. We measure the correlation-peak intensity value I_{cp} as

$$I_{\mathrm{cp}} = \iint_{A_p} |c(x, y)|^2 \mathrm{d}x\mathrm{d}y, \tag{3}$$

where A_p denotes the detector aperture and the total intensity of the light entering the CF plane I_f is

$$I_f = \iint |F'(u, v)|^2 \mathrm{d}u\mathrm{d}v. \tag{4}$$

From the measured quantities I_{cp} and I_f it is easy to calculate the similarity measure SM as

$$\mathrm{SM} = \frac{I_{\mathrm{cp}}}{I_f}, \tag{5}$$

and the discrimination ability DA as

$$\mathrm{DA} = \frac{\frac{1}{N}\sum_{i=1}^{N} \mathrm{SM}_i}{\max[|c(x, y)|^2]/I_f}. \tag{6}$$

In Eq. (6) the numerator represents the average SM of the in-class objects and the denominator is the maximum intensity in the correlation plane of an arbitrary object divided by the corresponding entering intensity.

3. Mathematical Model

Reducing the original 3-D information to 2-D data permits the resulting 2-D CI patterns to be described by the use of a simple mathematical model. The total set of the CI signs, S, is given by

$$S = \{s_n;\, n = 1, 2, \ldots, N\}, \tag{7}$$

where N is approximately equal to 600 for the Middle Babylonian epoch.[11] Although the considered set consists of a large number of elements, the way in which the signs are formed permits a relatively simple mathematical description. Each sign consists of a finite number of wedges of different sizes, rotations, and locations, i.e.,

$$s_n(x, y) = \sum_{i=1}^{I} \sum_{j=1}^{J_i} v(x_{ij}', y_{ij}') \otimes \delta(x - x_{0ij}, y - y_{0ij}), \tag{8}$$

where I is the number of possible rotations of a single wedge and J_i is the number of wedges with the ith rotation. The model is constrained by the requirement that each wedge be able to be described as a transformation of one basic wedge $v(x, y)$. The scale and rotation transformation can be expressed by a 2×2 square matrix, which is merely the transform of coordinates (x, y) into other coordinates (x_{ij}', y_{ij}'), i.e.,

$$\begin{bmatrix} x_{ij}' \\ y_{ij}' \end{bmatrix} = \begin{bmatrix} \sigma_{xij} \cos \alpha_i & \sigma_{yij} \sin \alpha_i \\ -\sigma_{xij} \sin \alpha_i & \sigma_{yij} \cos \alpha_i \end{bmatrix} \begin{bmatrix} x \\ y \end{bmatrix}, \tag{9}$$

where σ and α represent the scale and rotation parameters, respectively.

4. Coherent Optical Averaging

In this section an experimental method for realizing the average CF's by means of coherent optical processing is described. First, a coherent imaging system is aligned; the system consists of the input plane P_1', several small FT lenses placed in parallel, the FT plane P_2', one large FT lens, and the output plane P_3' (see Fig. 1). Suppose that the input amplitude distribution of such a system consists of N samples of in-class objects $s_i(x, y)$, with their positions arbitrarily distributed. By Fourier-transforming each sample independently and, in parallel, using small FT lenses, and by then using one large lens, we can record a joint-image hologram (JIH) at the output plane of the setup. With the assumption of linear recording, the amplitude transmittance of the developed photomaterial,

$$t(x, y) \propto \sum_{n=1}^{N} |s_n(x, y)|^2 + \sum_{n=1}^{N} \sum_{n \neq n, m=1}^{N} s_n(x, y) s_m^*(x, y) \times \exp\{-i2\pi[(u_n - u_m)x + (v_n - v_m)y]\}, \tag{10}$$

contains the desired first term on the right-hand side of proportion (10), as well as the intermodulation terms.

To record the average CF, the JIH is placed at the input plane P_1 of the correlator setup from Fig. 1. Taking the FT of the incident, coherent, collimated light modulated by the mask, the autocorrelation on-axis terms at plane P_2 are spatially separated from the cross-correlation off-axis terms. Thus, in the prefiltering stage (planes P_2 and P_3) all unwanted off-axis terms are filtered out, and the remainder is the sum of the sample intensities. For all inputs that can be described with real functions the squaring operation is of no importance. The resulting amplitude distribution is the average spectrum of the training objects, which is then Fourier transformed and holographically recorded at plane P_4 of the MEOC system. The filter function is obtained in the form

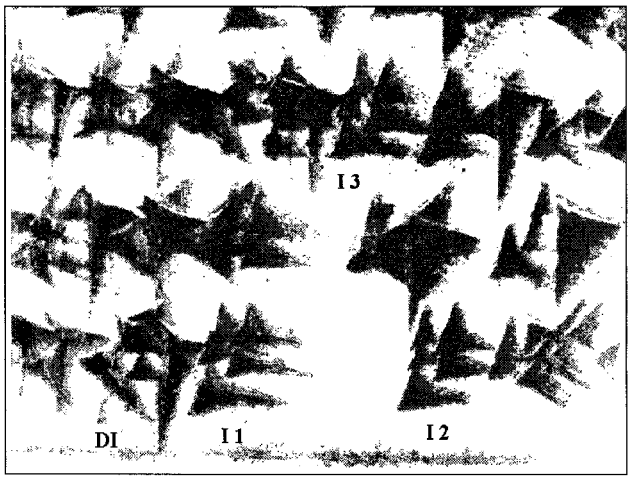

(a)

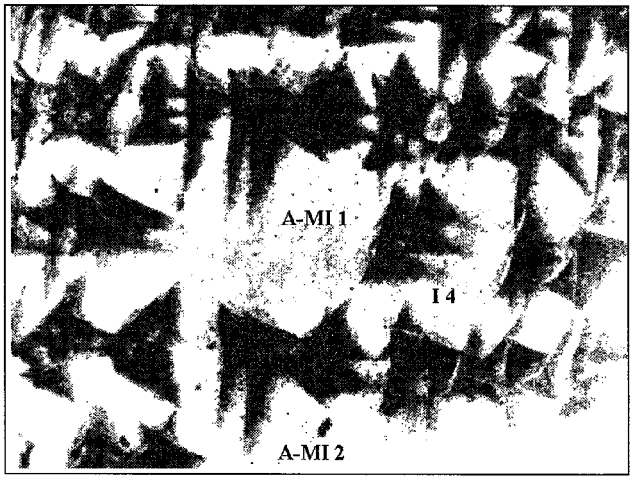

(b)

Fig. 4. Preprocessed input scenes: (a) scene 1 and (b) scene 2.

$$H^*(u, v) \propto \frac{1}{N} \sum_{n=1}^{N} \alpha_n S_n^*(u, v), \tag{11}$$

where α_n are the coefficients of a linear combination of N training objects.

5. Multifunctional System Algorithm

To understand better the procedures undertaken during the experimental work, the algorithm is sche-

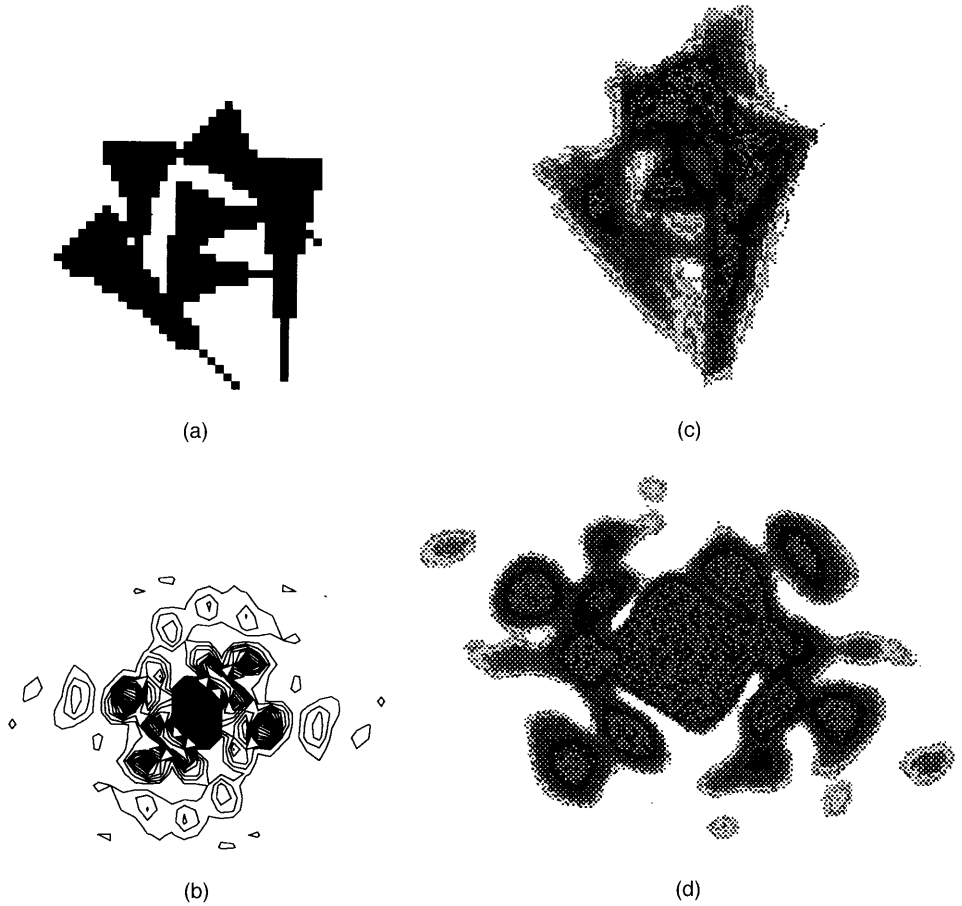

Fig. 5. Characterization of the DI sign: (a) the mathematical model, (b) the DI numerical power spectrum, (c) the preprocessed original DI_{av} sign, and (d) the optical power spectrum of sign DI_{av}.

matically shown in Fig. 2. The corresponding steps are given in following.

(A) Input Transparencies

1. Selecting the areas of interest on the original CI tablet by the use of the CCD camera and the DIP system. This steps also includes the dimension reduction (3-D $\rightarrow$ 2-D).
2. Selecting the in-class and out-of-class objects; digital preprocessing.
3. Isolating the training set of objects.
4. Recording the selected inputs on photographic film.

(B) Training-Set Features

1. Feature enhancement and feature extraction by the use of the extended optical Fourier-analysis and DIP systems.
2. Analysis of the training-set features in the object and Fourier domains.
3. Definition of various preprocessing parameters (e.g., the dimensions of cross stops in the FT plane and apertures in the image plane, the exposure parameters for QPOF masks, etc.).

(C) Preprocessing Procedures

1. Digital preprocessing (e.g., contrast enhancement, gray-scale level equilization, normalization, addition of images, etc.).
2. In-line optical spatial prefiltering in both the image and FT domains.
3. Implementation of coherent optical averaging of the selected set of in-class objects.
4. Synthesis of the power spectrum AM's for QPOF's.

(D) Correlation Filters: Optical Implementation of Various Types of CF's

1. CF's of single wedges.
2. CF's of single signs.
3. Multiplexed CF's of in-class single-sign models.
4. CF's of optically and digitally averaged in-class signs taken from the modeled CI tablet.
5. CF's of optically and digitally averaged in-class signs taken from the original CI tablet.
6. QPOF's (CF's recorded with the use of the AM) of optically and digitally averaged in-class signs taken from the original CI tablet.

(E) Cuneiform-Inscription Characterization Results

1. Characterization on the basis of both the object and the Fourier features.

2. Characterization on the basis of the correlation results.

6. Results

Figures 3(a) and 3(b) show photographs of the original tablet, HS 158b (Hilprecht–Sammlung Vorderasiatischer Altertümer Jena), from Nippur, 1329 B.C. It can be seen that the front side of the tablet is rather damaged, containing cracks and other defects that cause noise. Seven selected areas of interest were vertically illuminated, captured by a CCD camera, and stored in the DIP system memory. Two sets of in-class objects were formed, one consisting of I sign samples and the other of DI sign samples. One set of in-class objects $\{I_1, I_2, I_3, I_4\}$ and a selected set of out-of-class objects $\{DI, A\text{-}MI_1, A\text{-}MI_2\}$ in the contrast-enhanced scenes are indicated in Figs. 4(a) and 4(b). Three I signs, $\{I_1, I_2, I_3\}$, chosen to represent the training set, were then isolated and normalized to give the same total power. All selected and preprocessed inputs were then recorded on photographic film. Furthermore, the signs from the training set were used for synthesizing the average I pattern.

To implement experimentally the optical-averaging technique described in Section 4, we first organized a holder for the three I signs from the training set. The signs were placed in the input plane P_1' of the MEOC system shown in Fig. 1. Three parallel optical axes were formed with three small FT lenses, and consequently the spatially separated FT's appeared at plane P_2'. Because a large FT lens was used, the interference pattern of the three I signs was obtained at plane P_3'. The correct positioning of the small FT lenses was managed with the help of a special self-constructed carrier and by the observation of the overlapping pattern with the CCD camera and the DIP system. A JIH was then recorded by the use of standard photomaterials and photoprocessing. The next step was to introduce the JIH into plane P_1 of the MEOC system. By Fourier transforming the light passing through the JIH, we obtained three reconstructions for each I sign, of which one reconstruction for each sign was located on the optical axis of the system. Therefore, six reconstructed off-axis patterns were filtered out easily in the prefiltering stage of the MEOC system, while the on-axis overlapping patterns gave the average spectrum of the set $\{I_1, I_2, I_3\}$ at plane P_4 of the system.

Keeping the JIH as an input and simply recording only the part of the power spectrum at plane P_2 that was centered on the optical axis, we obtained the AM. Several AM's with different exposure times were recorded. The QPOF's were recorded holographically in plane P_4 of the MEOC system, with the JIH kept in the input plane and the AM selected and repositioned. Positioning the AM, as well as the CF, is a standard procedure with an accuracy requirement that is used for repositioning holograms; additionally, it was controlled by the use of the CCD camera and the DIP system. The correlation experiments were performed with and without the AM.

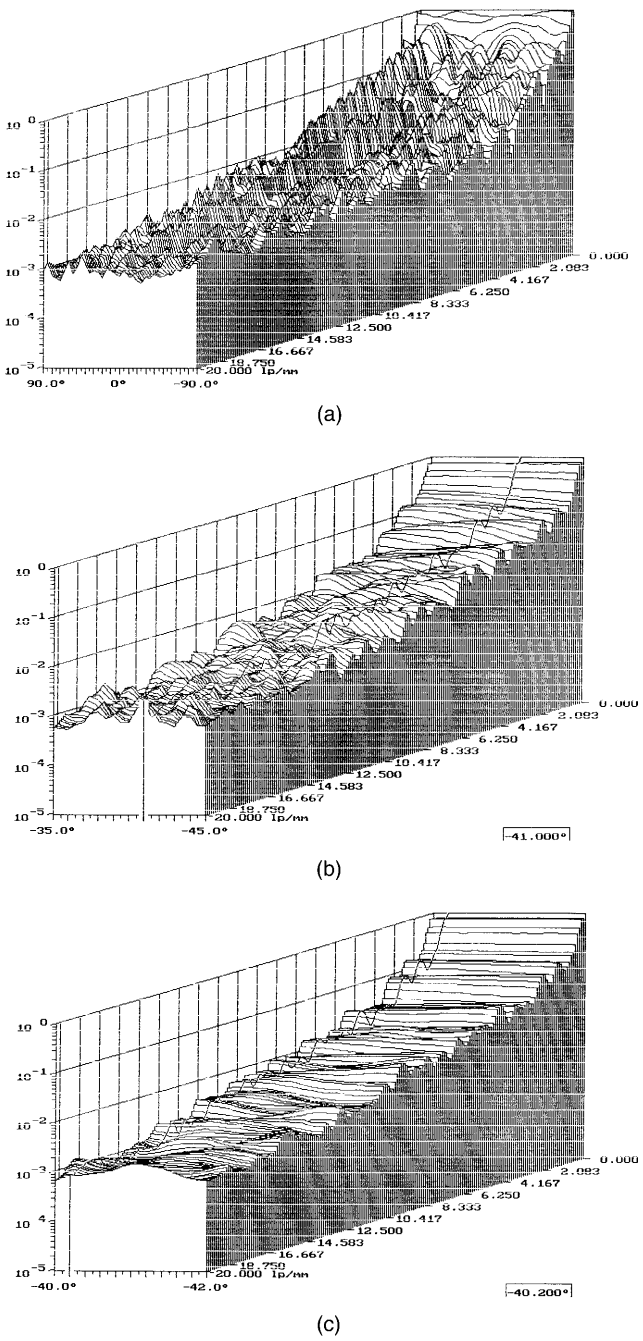

Fig. 6. Scans of (a) the FT structure of the DI sign over 180°, and (b) and (c) of selected finer intervals.

A. Features in the Object and Fourier Domains

The 2-D appearance of the CI signs depends on the illumination conditions applied to the CI tablet. With perpendicular illumination, the resulting 2-D objects look like those shown in Figs. 4(a) and 4(b). Such objects can be numerically described by the im-

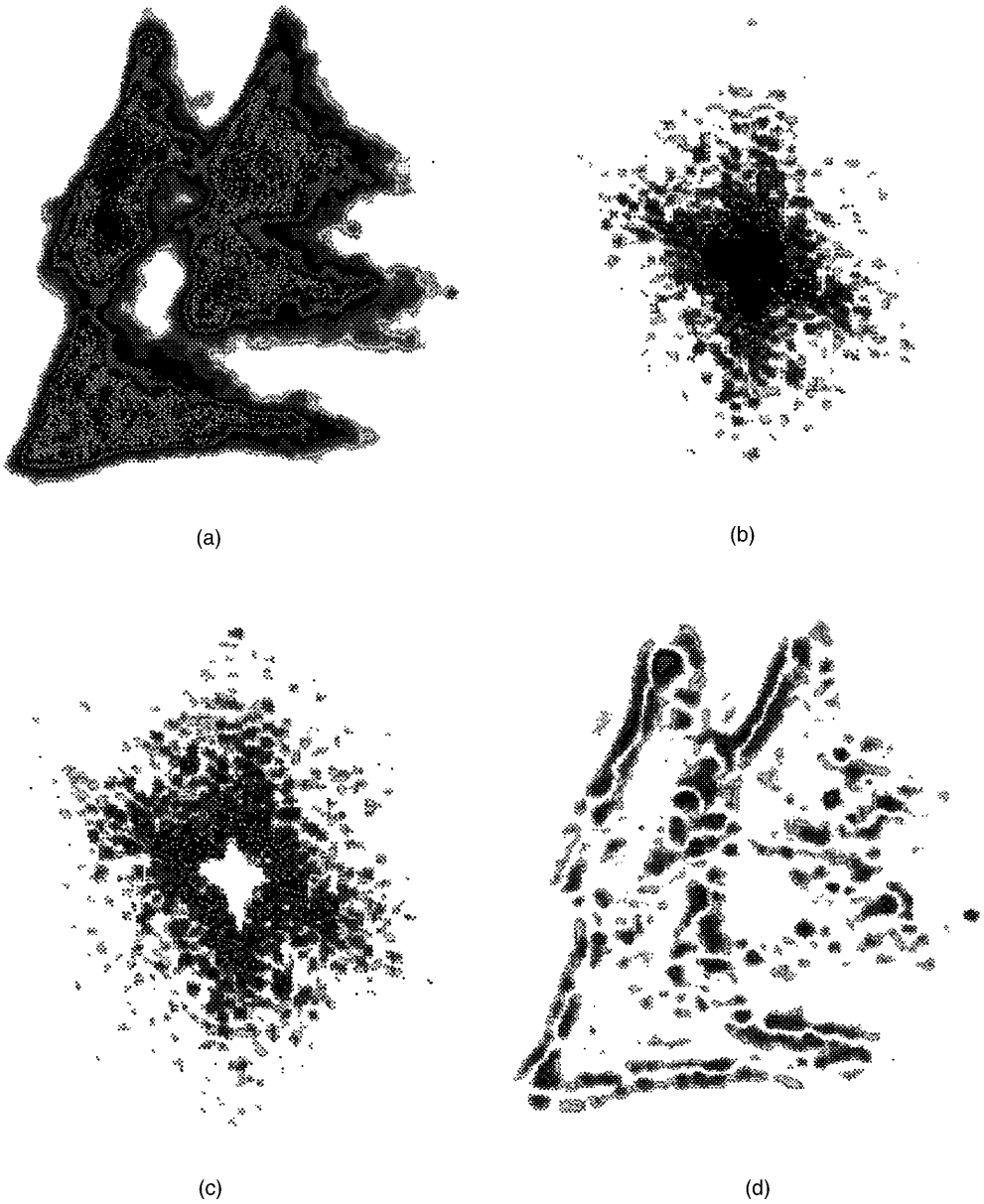

Fig. 7. Edge extraction by the use of an AM: (a) I_{av}, (b) I_{av} power spectrum, (c) results of the optical multiplication of the I_{av} power spectrum by an AM, and (d) the edge-extracted I_{av}.

plementation of the mathematical model presented in Section 3 on 64 × 64 arrays. According to our model, any CI sign can be described by Eq. (8) in terms of the transformation parameters I, J, σ, α, and (x_0, y_0). For example, the DI sign is defined with $I = 3$, $J = \{2, 2, 2\}$, $\sigma = \{(1, 0.5), (1, 0.5), (1, 0.75), (1, 1), (1, 0.6), (1, 1)\}$, $\alpha = \{0, -\pi/4, -\pi/2\}$, and locations in pixels (x_0, y_0) have the values $(x_0, y_0) = \{(29, 41), (36, 40), (20, 35), (33, 20), (31, 24), (33, 42)\}$ [see Fig. 5(a)]. The numerical power spectrum for DI is shown in Fig. 5(b). For comparison, Figs. 5(c) and 5(d) show the DI average and its optical power spectrum, respectively.

Another approach to characterization in the FT domain is demonstrated in Figs. 6(a)–6(c) with an example of one sample of the DI sign. Figure 6(a) shows a 180° scan from 0 to 20 line pairs/mm obtained with a photodiode detector that is controlled by a PC and driven by stepping motor. Comparing the area integrals makes it possible to select the powerful lines and the corresponding angles. A selected angle interval between −35° and −45° is shown in Fig. 6(b). Insight into a more detailed structure is possible by the selection of smaller angle intervals, as illustrated in Fig. 6(c) for the angle interval between −40° and −42°.

B. Correlation Experiments

In this section we show the similarity measures between the optically averaged object I_{av} and the pre-

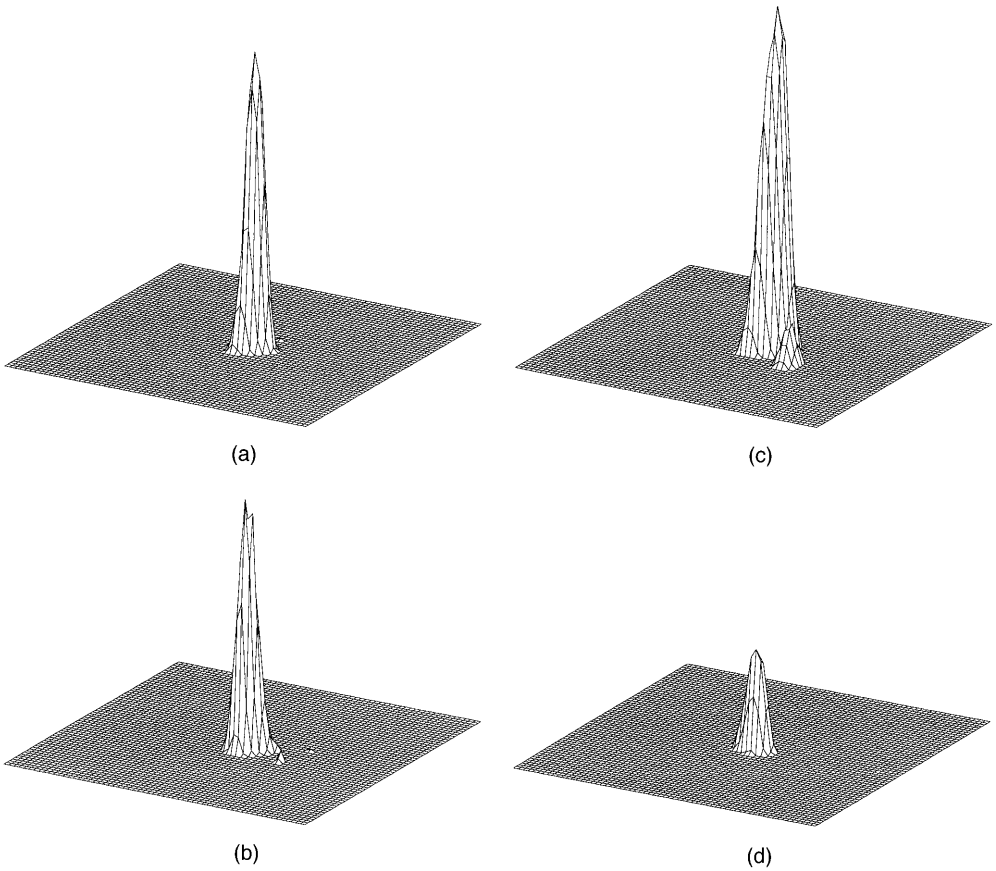

Fig. 8. Correlation output obtained by the use of an AM: I_{av} is correlated with (a) I_1, (b) I_2, (c) I_3, and (d) I_4.

viously selected objects: in-class objects $\{I_1, I_2, I_3, I_4\}$, where $\{I_1, I_2, I_3\}$ represents the training set, and out-of-class objects $\{DI_1, DI_2, DI_3, A\text{-}MI_1, A\text{-}MI_2\}$. For performing correlation experiments, the QPOF's of I_{av} were made according to the procedure described in Subsection 2.B and above in this section. First we demonstrate the role of the AM in Fig. 7. Figures 7(a) and 7(b) show the input object I_{av} at plane P_1 and its power spectrum at plane P_2 of the MEOC system, respectively. The effect of multiplication of the spectrum in Fig. 7(b) by the AM is shown in Fig. 7(c). Obviously, an edge-extraction operation is achieved, and the bandpass FT of I_{av} shown in Fig. 7(d) was used for synthesizing the QPOF's. During the correlation experiments, the AM can be either retained or removed. The correlation results are shown in Figs. 8(a)–8(d) with the AM, and in Figs. 9(a)–9(i) without the AM. From these plots it is readily seen that the resulting output signals are much wider when the AM is removed. Comparing the average SM corresponding to the correlations shown in Figs. 8 with the respective average SM of Figs. 9, we obtain a ratio of 0.11, which can easily be calculated from Table 1, in which the data are normalized to the maximum SM. The SM of the in-class, out-of-training-set object I_4 was 36% of the average SM from the training set with the AM versus 54% without the AM. The DA values were also compared. The re-

Table 1. Normalized Similarity Measures SM

Input Objects	SM: With an AM	SM: Without an AM
In class		
I_1	0.089	0.859
I_2	0.076	0.627
I_3	0.103	1.000
I_4	0.032	0.446
Out of class[a]		
DI_1	0.013	0.179
DI_2	0.012	0.288
DI_3	0.006	0.250
$A\text{-}MI_1$		0.224
$A\text{-}MI_2$		0.167

Table 2. Average Discrimination Ability DA Values

Input Objects	SM: With an AM	SM: Without an AM
In class		
I_1, I_2, I_3	1.0	1.0
I_4	2.8	1.9
Out of class[a]		
DI_1, DI_2, DI_3	8.7	3.5
$A\text{-}MI_1, A\text{-}MI_2$		4.2

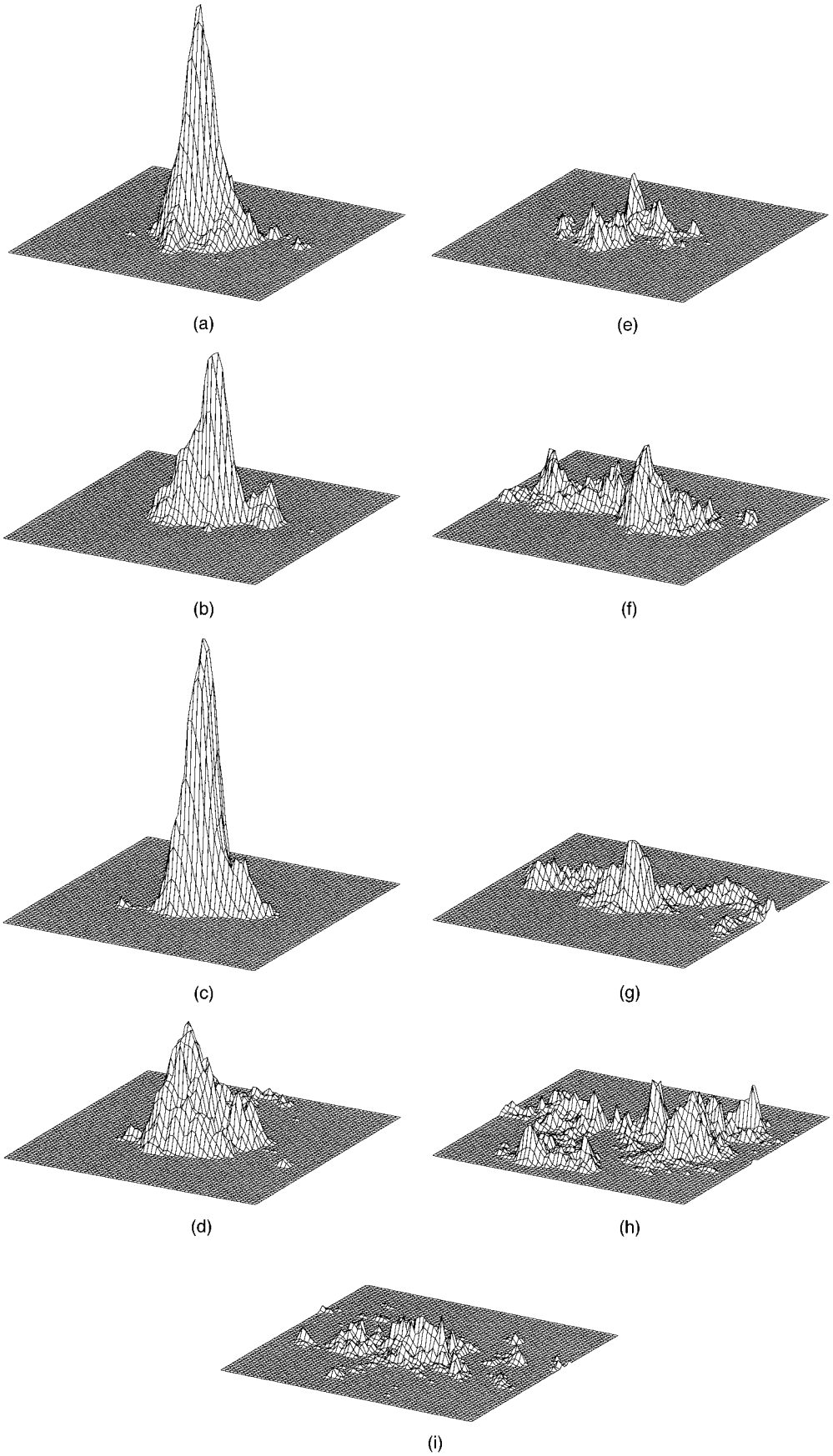

Fig. 9. Correlation output obtained without the use of an AM: I_{av} is correlated with (a) I_1, (b) I_2, (c) I_3, (d) I_4, (e) DI_1, (f) DI_2, (g) DI_3, (h) A-MI_1, and (i) A-MI_2.

sults presented in Table 2 show a much higher sensitivity for the SM when the AM is applied during correlation experiments. For example, the DA for the out-of-class $\{DI_1, DI_2, DI_3\}$ objects was equal to 8.7 with the AM versus 3.5 without the AM.

7. Summary and Conclusions

To characterize the CI signs a multifunctional optoelectronic device was advanced that permits detection, Fourier analysis, feature enhancement, feature extraction, coherent optical averaging, and correlation experiments to be performed, including various preprocessing procedures. A block diagram of the overall algorithm and the corresponding experimental steps are also provided. Preliminary characterization results are given for several CI signs recorded on the original clay tablet from Nippur, 1329 B.C.

To describe the CI signs numerically, a simple 2-D mathematical model is introduced that is based on describing a CI sign as a linear combination of both scale and rotation transformations of an elementary wedge. Thus, it was possible to emulate features of approximately 600 CI signs belonging to the Middle Babylonian epoch. Alternatively, the features in the FT space of the preprocessed CI signs were measured along radial spatial-frequency components for selected gradual angle intervals. To decrease the sensitivity between different samples of a sign, we designed and implemented a coherent optical technique for averaging in-class objects. For increasing the diffraction efficiency of the CF's, the QPOF's have been synthesized and the corresponding correlation outputs quantified.

Used as described in this paper, the technique of coherent optical averaging is time consuming because the small FT lenses must be adjusted by hand or photographic plates must be used for recording the QPOF's and AM's. Our future research will be aimed at improving such adjustment procedures and include optically or electronically addressable spatial light modulators instead of photographic emulsions.

Although applied to a statistically small sample, the developed experimental device and techniques have been demonstrated to be a possible solution to the CI characterization problem. A detailed investigation involving many more samples is under preparation.

This work was performed at the Institute of Physics, Humboldt University of Berlin, Germany. The authors are grateful to the Bundesministerium für Bildung, Wissenschaft, Forschung und Technologie for financial support under contract 03-WE9HUB. N. Demoli is grateful to the German Academic Exchange Service (DAAD) for financial support. The authors are also thankful to S. Boseck and L. Begemann (University of Bremen), G. von Bally, A. Roshop, and F. Dreesen (University of Münster), and the reviewers of the manuscript for their contributions to this paper.

References

1. A. VanderLugt, "Signal detection by spatial complex filtering," IEEE Trans. Inf. Theory **IT-10,** 139–145 (1964).
2. J. M. Fournier, "Coherent and incoherent averaging of ancient handwritten hebraic characters," in *Applications of Holography and Optical Data Processing*, E. Marom, ●●●, eds., (Pergamon, London, 1977), pp. 533–540.
3. J. Duvernoy and Y.-L. Sheng, "Effective optical processor for computing image moments at TV rate: use in handwriting recognition," Appl. Opt. **26,** 2320–2327 (1987).
4. T. S. Wilkinson, D. A. Pender, and J. W. Goodman, "Use of synthetic discriminant functions for handwritten-signature verification," Appl. Opt. **30,** 3345–3353 (1991).
5. B.-S. Jeng, "Optical Chinese character recognition using accumulated stroke features," Opt. Eng. **28,** 793–799 (1989).
6. G. von Bally, D. Vukičević, N. Demoli, H. Bjelkhagen, G. Wernicke, U. Dahms, H. Gruber, and W. Sommerfeld, "Holography and holographic pattern recognition for preservation and evaluation of cultural-historic sources," Naturwissenschaften **81,** 563–565 (1994).
7. N. Demoli, H. Gruber, U. Dahms, and G. Wernicke, "Holographic technique application in analysing cuneiform inscriptions," J. Mod. Opt. **42,** 191–195 (1995).
8. N. Demoli, U. Dahms, H. Gruber, and G. Wernicke, "Use of a multifunctional extended optical correlator for cuneiform inscription analysis," in *Photonics for Processors, Neural Networks, and Memories II*, J. L. Horner, B. Javidi, and S. T. Kowel, eds., Proc. SPIE **2297,** 278–287 (1994).
9. C. B. F. Walker, *Cuneiform* (Trustees of the British Museum, London, 1987).
10. N. Demoli, "Quasiphase-only matched filtering," Appl. Opt. **26,** 2058–2061 (1987).
11. R. Labat, *Manual D'Epigraphie Akkadienne* (Librairie Orientaliste Paul Guethner, S.A., Paris, 1977).